AAS 25-220

OPTIMIZATION OF WEAK STABILITY BOUNDARY TRANSFERS UNDER UNCERTAINTY: THE LUMIO MISSION CASE

Alessandro Martinelli[*], Carmine Buonagura[†], Carmine Giordano[‡] and Francesco Topputo[§]

The rise of CubeSats has highlighted the need for mission analysis that integrates uncertainties inside the optimization phase. This work incorporates uncertainties in initial conditions, maneuvers, and navigation into a stochastic trajectory optimization process. It uses a novel implementation of the unscented transformation, avoiding sigma points resampling by employing a continuous propagation map. The problem is formulated as a nonlinear programming problem and applied to weak stability boundary trajectories, with the LUMIO mission as a case study. The method yields more fuel-efficient and robust trajectories compared to deterministic optimization. Monte Carlo analyses validate the effectiveness and accuracy of the approach.

INTRODUCTION

Traditionally, space mission analysis follows a sequential approach, where a nominal trajectory is first optimized, and the effects of uncertainties on space flight are evaluated afterward, with a comprehensive navigation analysis.[1] These uncertainties stem from three main sources: actuation errors (differences between intended and actual thrust), navigation errors (differences between true and estimated trajectory), and dynamics model errors (differences between the model and actual space environment).[2] Additionally, errors from the launcher on the orbit injection impact the initial conditions of the trajectory. The output of the sequential approach is sub-optimal, as only the nominal ΔV is optimized, whereas the navigation ΔV is not. While this method works for large spacecraft with significant control authority, it becomes problematic for smaller missions, like those using CubeSats. CubeSats, due to their limited propulsion systems and low navigation capabilities,[3] have a low-control authority, and are thus more susceptible to the effects of uncertainties during space flight . Modern advances in astrodynamics have also introduced missions in highly perturbed environments, such as the Earth–Moon weak stability boundary (WSB)[4] transfers, further complicating the impact of uncertainties.

Therefore, nowadays researchers are increasingly focusing on optimizing trajectories under uncertainty. However, incorporating uncertainties inside the optimization phase is not an easy task.

[*]Ph.D. Student, Department of Aerospace Science and Technology, Politecnico di Milano, Via La Masa 34, Milan 20156, Italy. alessandro2.martinelli@polimi.it

[†]Ph.D. Student, Department of Aerospace Science and Technology. Politecnico di Milano, Via La Masa 34, Milan 20156, Italy, carmine.buonagura@polimi.it

[‡]PostDoc Fellow, Department of Aerospace Science and Technology, Politecnico di Milano, Via La Masa 34, Milan 20156, Italy. carmine.giordano@polimi.it

[§]Full Professor, Department of Aerospace Science and Technology, Politecnico di Milano, Via La Masa 34, Milan 20156, Italy. francesco.topputo@polimi.it

Indeed, any form of randomness will jeopardize the solution of the problem with the conventional numerical methods used in trajectory optimization.[5] To avoid that, one possibility is to consider an appropriate uncertainty propagation method,[6] so that the stochastic optimization problem can be transformed into a deterministic one, and thus solved conventionally. Different uncertainty propagation techniques can be used. For example, linear covariance propagation has been used to obtain robust trajectories by optimizing correction maneuvers under the effect of execution errors and process noise in the dynamics.[7] The unscented transformation (UT) has been used to optimize interplanetary transfers, under the effect of navigation errors and noisy dynamics,[8,9] or in low-thrust trajectory optimization problems, using stochastic differential dynamic programming.[10] To optimize guidance policies for orbits around small bodies, UT and linear propagation methods have been used together.[11] In addition, in stochastic trajectory optimization problems, often hard constraints are reformulated as chance constraints, i.e., constraints on the probability of exceeding a certain threshold.[12] General procedures for integrating the navigation assessment inside the optimization phase have been also proposed, by exploiting the polynomial chaos expansion in the cislunar region,[13] or by developing the belief optimal control problem, applied to flyby trajectories.[14] Also the problem of the optimal station-keeping on unstable libration-point orbits has been considered from a stochastic perspective.[15]

In this paper, a new method for optimizing space flight trajectories under uncertainty with impulsive maneuvers is presented. It considers uncertainties from initial conditions, maneuvers execution errors, and navigation errors. The approach minimizes the cost of both nominal and correction maneuvers while respecting stochastic constraints on the final covariance matrix. The unscented transformation is employed to propagate uncertainties, translating the stochastic problem into a deterministic nonlinear programming (NLP) problem. This method improves upon previous work by using a continuous propagation map, in which trajectories and uncertainties are propagated simultaneously, avoiding the need of resampling sigma points at each maneuvering time. This avoids the oversimplification of assuming that the distribution remains normal during the propagation. In addition, for the first time a stochastic optimization is applied to a WSB transfer trajectory, using the LUMIO mission as a test case.[16] Results show that the new method produces more robust nominal trajectories that require less fuel compared to traditional deterministic approaches. Finally, Monte Carlo simulations validate the effectiveness of the method.

The paper is organized as follows: first, a brief introduction on LUMIO mission analysis is given, focusing on the dynamical model, the nominal trajectory, and the navigation assessment; then, the new methodology for stochastic optimization is explained; afterwards, numerical results are given and validated with Monte Carlo simulations; finally, conclusions on the effectiveness of the method are provided.

INTRODUCTION TO LUMIO MISSION ANALYSIS

LUMIO, which stands for LUnar Meteoroid Impacts Observer, is a 12U CubeSat mission to a halo orbit around the Earth–Moon L_2 point. From this vantage position, LUMIO will observe, quantify, and characterize the impacts of meteoroids on the lunar far side, which is always visible from the halo orbit. To do that, LUMIO is equipped with the LUMIO-Cam, an optical camera to detect the light flashes coming from the meteoroid impacts with the lunar surface. The operational orbit for the mission, which is shown in Figure 1, is a quasi-halo orbit generated in an ephemerides model from the ideal halo in the CR3BP, with a Jacobi Constant of 3.09. The selection of this particular orbit is the result of a trade-off performed during phase 0.[17] Regarding the transfer trajectory, from

phase B onwards, LUMIO is expected to fly on a weak stability boundary trajectory to get to its operational orbit. A comprehensive review of the methodologies and results of the WSB trajectory design and optimization for the LUMIO mission has been already presented by the authors.[18]

The LUMIO mission analysis has followed a sequential approach, where a nominal trajectory is designed and optimized first, and then a stochastic analysis is performed. In this section we will not focus on the whole process, which would require a standalone article by itself. Instead, we will introduce some aspects that will be taken into account later on the stochastic trajectory optimization problem, which is the focus of this work. First, the dynamical model in which the computations are performed is presented. Then, the results of the conventional, deterministic optimization process are given. In particular, the characteristic of the nominal WSB trajectories are presented. Finally, the navigation assessment performed on these trajectories is introduced.

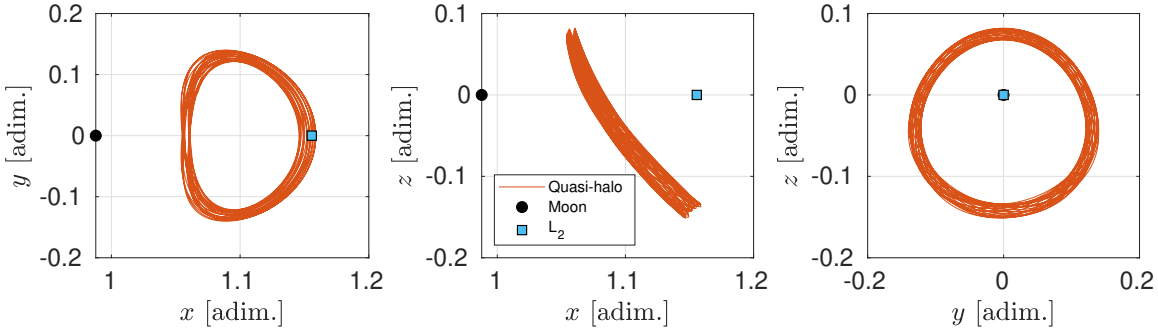

Figure 1: LUMIO Operational Orbit

Dynamical Model

The dynamical model for LUMIO is the roto-pulsating restricted n-body problem (RPRnBP).[19] This is an ephemeris-based model of the Solar System, written as an extension of the CR3BP. Indeed, the reference frame is built to rotate and pulsate together with a couple of primaries, here the Earth and the Moon, similarly to what is usually done in the CR3BP. The origin of the frame is on the primaries barycenter, the x-axis goes form the bigger body to the secondary body, the z-axis is aligned with their angular momentum, and the y-axis completes the right-hand frame. To build the roto-pulsating frame a time-dependent conversion from the inertial frame is needed.[20] Then, using the Lagrangian formalism, the equations of motion can be obtained.[21] These are usually normalized as in the CR3BP normalization convention.[22] The normalized equations of motion are:

$$\begin{aligned} \boldsymbol{r}'' = &-\frac{2}{n}\left(\frac{\dot{k}}{k}I + C^T\dot{C}\right)\boldsymbol{r}' - \frac{1}{n^2}\left[\left(\frac{\ddot{k}}{k}I + 2\frac{\dot{k}}{k}C^T\dot{C} + C^T\ddot{C}\right)\boldsymbol{r} + \frac{1}{k}C^T\ddot{\boldsymbol{b}}\right] + \\ &+ G\frac{m_1+m_2}{n^2k^3}\left[(1-\mu)\frac{\boldsymbol{r}-\boldsymbol{r}_1}{\|\boldsymbol{r}-\boldsymbol{r}_1\|^3} + \mu\frac{\boldsymbol{r}-\boldsymbol{r}_2}{\|\boldsymbol{r}-\boldsymbol{r}_2\|^3} + \sum_j \hat{\mu}_j\frac{\boldsymbol{r}-\boldsymbol{r}_j}{\|\boldsymbol{r}-\boldsymbol{r}_j\|^3}\right] + \boldsymbol{a}_{SRP} \end{aligned} \tag{1}$$

where: the symbols $(\,')$ and $(\,\dot{})$ are used for a derivative with respect to the non-dimensional and dimensional time, respectively; $\boldsymbol{r}$, $\boldsymbol{r}_1$, $\boldsymbol{r}_2$ and $\boldsymbol{r}_j$ are the position vectors of the spacecraft, the primaries and the remaining j bodies, in the roto-pulsating frame; n is the mean motion of the primaries; k is the time-dependent distance between the primaries; C is the rotation matrix between the inertial frame centered on the solar system barycenter and the roto-pulsating frame; I is the

identity matrix; $\boldsymbol{b}$ is the position vector of the primaries barycenter in the inertial frame; G is the gravitational constant; m_1 and m_2 are the masses of the primaries; $\mu = \frac{m_2}{m_1+m_2}$ is the mass fraction; $\hat{\mu}_j = \frac{m_j}{m_1+m_2}$; $\boldsymbol{a}_{SRP}$ is the normalized acceleration due to solar radiation pressure (SRP). The SRP acceleration is modeled using the cannonball model. Thus:

$$\boldsymbol{a}_{SRP} = \frac{1}{kn^2} \frac{c_r A P_0}{m} \frac{d_0^2}{d^2} \frac{\boldsymbol{r} - \boldsymbol{r}_S}{\|\boldsymbol{r} - \boldsymbol{r}_S\|} \tag{2}$$

where $\frac{1}{kn^2}$ is the normalization coefficient, c_r is the reflectivity coefficient of the spacecraft, A is the illuminated area of the spacecraft, m is the spacecraft mass, P_0 is the constant reference pressure at a distance d_0, while d is the current distance from the Sun, whose position vector in the roto-pulsating frame is $\boldsymbol{r}_S$.

When integrating the equations of motion, the position of the celestial bodies are given by the JPL ephemerides DE432,[23] which are retrieved with the SPICE toolkit.[24,25]

Nominal Trajectories

LUMIO is expected to be launched on a ride-share opportunity, on a WSB trajectory towards the Moon. Half a day after the trans lunar injection (TLI), LUMIO will be released; after this, it will count on its own propulsion to deviate the trajectory towards the quasi-halo orbit. A maximum of 8 deep space maneuvers (DSM) are foreseen, even though on average only 2 are needed. At the end of the transfer, an halo insertion maneuver (HIM) will be performed. For phase B, one transfer per week for the year 2027 has been computed, with pre-assigned fixed launch conditions, for a total of 52 trajectories. Nominal trajectories are numbered with the week of the year. The transfer nominal ΔV trend over the year can be seen in Figure 2a, where an average cost of around 40 $\mathrm{m/s}$ can be noticed. The baseline trajectory, i.e., trajectory #20, is shown in Figure 2b, together with the positions of the TLI, the release, the DSMs (only 2 in this case), and the final HIM.

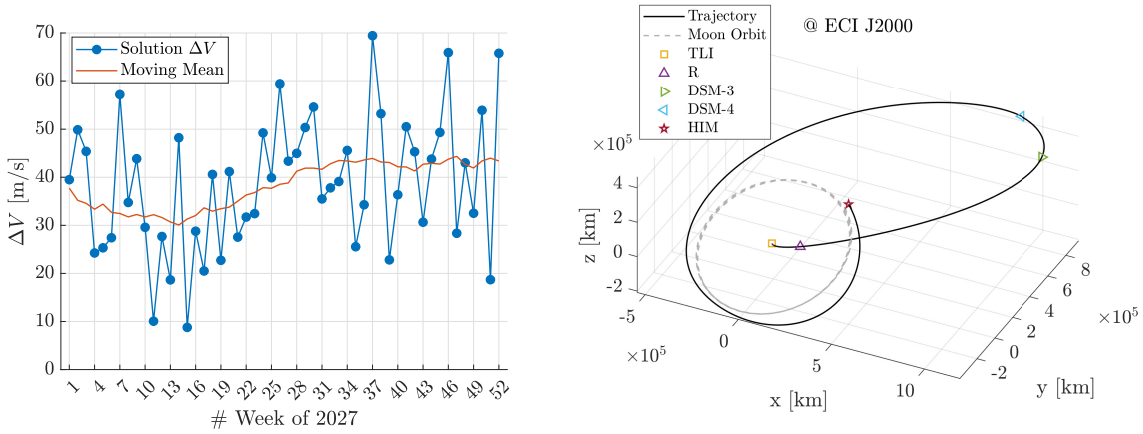

(a) Nominal Transfers ΔV

(b) LUMIO WSB Transfer Trajectory #20

Figure 2: Nominal Trajectory Optimization Results

Navigation Assessment

The navigation assessment performed for LUMIO mission analysis is composed of a knowledge and a dispersion analysis. The knowledge represents the stochastic difference between the estimated

trajectory, coming from the orbit determination (OD) or navigation process, and the real one. The dispersion instead, is the stochastic difference between the true trajectory and the nominal one. The uncertainties affecting the trajectory are: the the initial conditions, maneuvers execution errors, navigation errors, and process noise in the dynamics. To control the dispersion, trajectory correction maneuvers (TCMs) are planned. On average a TCM is planned every 7-10 days, also in simultaneity with the DSMs, and are almost equally distributed in time. Each TCM is computed with the *differential guidance* strategy.[26] In this strategy, two consecutive correction maneuvers are applied to cancel both the position and the velocity deviations on the final maneuvering point. However, the final impulse is usually not applied in practice, since at the final point a new maneuver is calculated in a receding horizon approach. Thus, the maneuver can be computed by minimizing the deviations from the nominal state at the final point in a least square residual sense. The maneuver applied at the time t_k, in order to cancel out the deviations at time t_{k+1}, is:[26]

$$\Delta \boldsymbol{v}_k = -\left(\boldsymbol{\Phi}_{rv}^T \boldsymbol{\Phi}_{rv} + q\boldsymbol{\Phi}_{vv}^T \boldsymbol{\Phi}_{vv}\right)^{-1} \left(\boldsymbol{\Phi}_{rv}^T \boldsymbol{\Phi}_{rr} + q\boldsymbol{\Phi}_{vv}^T \boldsymbol{\Phi}_{vr}\right) \delta \boldsymbol{r}_k - \delta \boldsymbol{v}_k \tag{3}$$

where $\boldsymbol{\Phi}_{rr}$, $\boldsymbol{\Phi}_{rv}$, $\boldsymbol{\Phi}_{vr}$, and $\boldsymbol{\Phi}_{vv}$ are the 3-by-3 blocks of $\boldsymbol{\Phi}(t_k, t_{k+1})$, i.e., the state transition matrix (STM) of the nominal trajectory from t_k to t_{k+1}, while $\delta \boldsymbol{r}$ and $\delta \boldsymbol{v}$ are the deviations of the estimated trajectory with respect to the nominal trajectory.

Regarding the knowledge analysis, the navigation of LUMIO has been simulated considering range and range-rate from the Cebreros ground station. Starting from an initial knowledge, the covariance matrix is propagated linearly up to the time of OD. During OD, pseudo-measurements are generated and are then employed in an extended kalman filter (EKF)[27] to estimate the state vector of the spacecraft, and reduce the covariance matrix. At the time of DSMs, uncertainty in the maneuver is added to the covariance matrix. Both the state and the covariance matrix are propagated with the associated dynamics up to each measurement epoch, where the state estimates are sequentially updated, leading to the position and velocity knowledge profiles. The dispersion analysis, instead, is based on a Monte Carlo simulation of the possible true trajectories, whose distance from the nominal constitutes the dispersion. Starting from an initial Gaussian distribution, a set of initial conditions is generated. Each sample is propagated forward, considering the deterministic accelerations plus the process noise associated to the solar radiation pressure and the residual acceleration. Integration is performed with the hybrid stochastic-deterministic integrator, labeled Euler-Maruyama-Runge-Kutta (EMRK).[28] The propagation of each sample corresponds to a possible true trajectory. At the final time of orbit determination, the estimated state is simulated by adding to the true state the navigation error coming from the knowledge analysis. Propagation of the estimated trajectory is used in the guidance scheme, while the actual TCM is applied on the true trajectory. The following are a list of assumptions used for both knowledge and dispersion analysis:

- The initial knowledge and dispersion at the time of LUMIO release is equal to 100 km for position components and 0.05 m/s for velocity components.
- A thrust error of 2% in magnitude and 1.5 deg in direction (1σ) is considered only on DSMs. The error on TCMs is considered to be negligible, and is thus discarded.
- The OD is simulated only on the nominal trajectory, without loss of generality.
- A cut-off time (COT) of 2 days is considered before maneuvers.
- A window of 1 day is considered to perform OD before the COT.

- SRP and residual acceleration are modeled as Gauss–Markov (GM) processes, whose characteristics are listed in Table 1.

Table 1: Gauss–Markov Processes Characteristics

Gauss–Markov Process	σ	τ
Solar Radiation Pressure	5% in magnitude	1d
Residual Acceleration	10^{-12} km/s^2	1d

The results of the knowledge and dispersion analysis are shown in Figure 3 and 4, both for trajectory #20. Results on the other trajectories are similar, and in general show that the trajectory can be controlled within the proposed approach and assumptions. However, the cost for this control, label navigation ΔV, can be relevant, as on average it is the 60% of the nominal transfer cost. This, in addition to the station-keeping cost, disposal, and required margins, makes some of the trajectories exceed the total ΔV budget limit of 80 m/s, as it can be seen in Figure 5. This highlights that the sub-optimality of the sequential approach adopted up to now in the LUMIO mission analysis, is not acceptable. On the contrary, an integrated approach, where a stochastic optimization of the trajectory is performed, may be useful in reducing the ΔV budget for the mission.

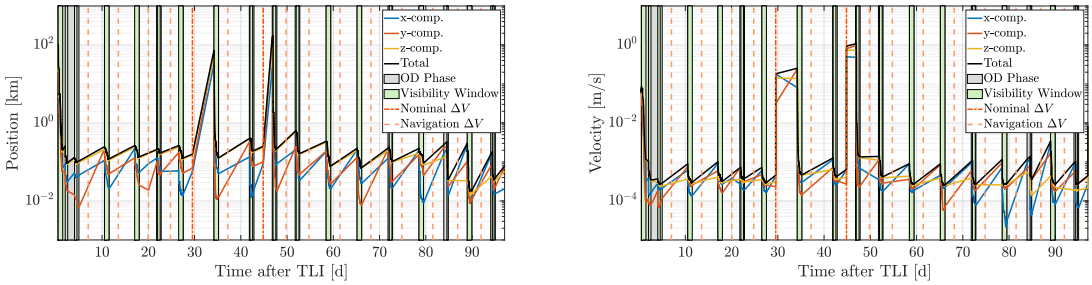

(a) 1σ Position Knowledge

(b) 1σ Velocity Knowledge

Figure 3: Knowledge Analysis Results

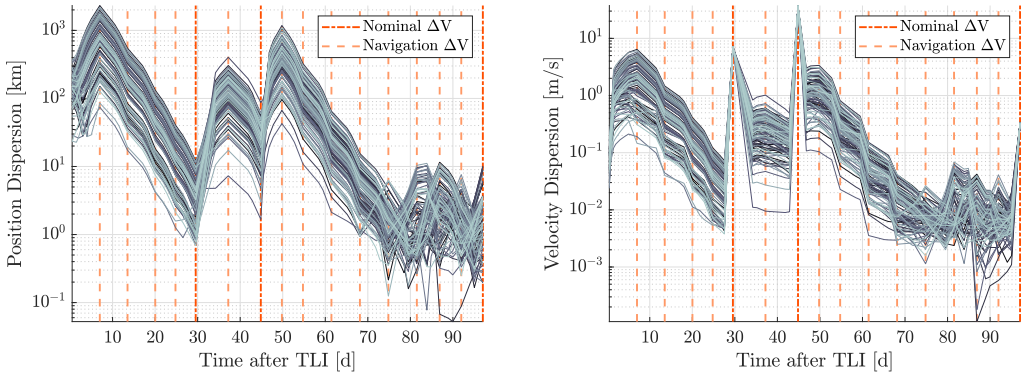

(a) Monte Carlo Samples Position Dispersion

(b) Monte Carlo Samples Velocity Dispersion

Figure 4: Dispersion Analysis Results

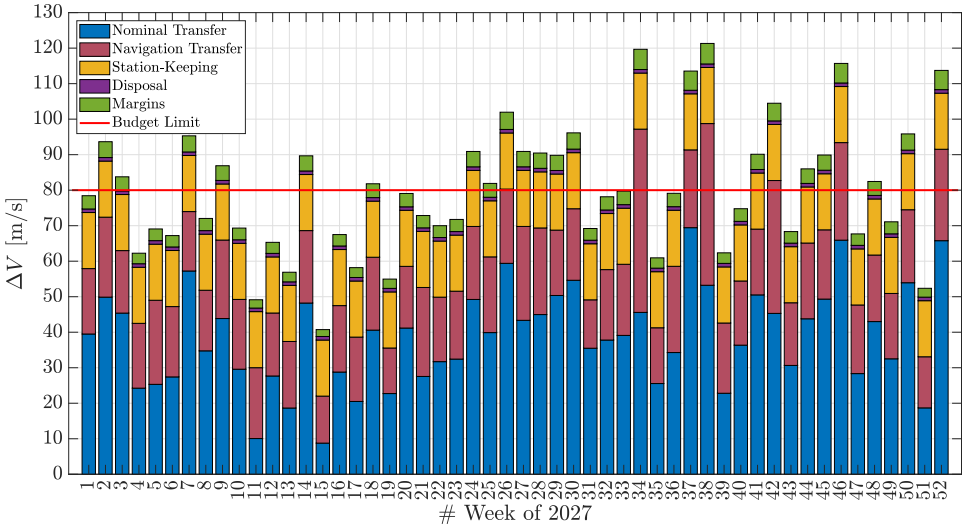

Figure 5: LUMIO ΔV Budgets

STOCHASTIC TRAJECTORY OPTIMIZATION PROBLEM

In this section, the stochastic trajectory optimization problem is formulated, and the methodology is presented. Although the idea to optimize trajectories in a stochastic way stems directly from the needs of the LUMIO mission analysis, nonetheless the developed methodology is general, and can be effortlessly applied to other scenarios.

Methodolgy

In this section the procedure for the the propagation with the unscented transformation is explained. First, the trajectory is discretized in $n+1$ time intervals: $t_0, t_1, \ldots, t_k, \ldots, t_n$. At time t_0 initial conditions $\boldsymbol{x}_0$ are modelled as a Gaussian random variable: $\boldsymbol{x}_0 \sim \mathcal{N}(\overline{\boldsymbol{x}}_0, \boldsymbol{P}_0)$. In addition to the initial conditions, the other sources for uncertainty are the maneuver execution errors and the navigation errors. Regarding the first type of errors, these are assumed to be present only on the DSMs, thus excluding the TCMs, as it was done previously. DSMs are modeled as Gaussian random variables: $\Delta\boldsymbol{v}_{DSM} \sim \mathcal{N}\left(\overline{\Delta\boldsymbol{v}}_{DSM}, \boldsymbol{P}_{DSM}\right)$. The uncertainty comes from errors on the thrust magnitude, $\sigma_{\Delta v}$, and on the pointing angle, σ_δ. The TCMs are, instead, directly affected by the navigation error. A single navigation error is considered for all TCM times and it is modeled as a Gaussian random variable: $\boldsymbol{\varepsilon}_{OD} \sim \mathcal{N}(\boldsymbol{0}, \boldsymbol{P}_{OD})$. Finally, dynamical model errors are not considered inside the optimization, but are considered in the validation phase as Gauss–Markov processes to be added in the dynamics. All uncertainties are collected in a single vector of dimension N, $\boldsymbol{\mathcal{X}}_0$, defined as:

$$\begin{aligned} \boldsymbol{\mathcal{X}}_0 \sim \mathcal{N}\left(\overline{\boldsymbol{\mathcal{X}}}_0, \boldsymbol{\mathcal{P}}_0\right) &= \left[\boldsymbol{x}_0, \Delta\boldsymbol{v}_{DSM-1}, \Delta\boldsymbol{v}_{DSM-2}, \ldots, \boldsymbol{\varepsilon}_{OD}\right]^T \\ \overline{\boldsymbol{\mathcal{X}}}_0 &= \left[\overline{\boldsymbol{x}}_0, \overline{\Delta\boldsymbol{v}}_{DSM-1}, \overline{\Delta\boldsymbol{v}}_{DSM-2}, \ldots, \overline{\boldsymbol{\varepsilon}}_{OD}\right]^T \\ \boldsymbol{\mathcal{P}}_0 &= \text{diag}\left(\boldsymbol{P}_0, \boldsymbol{P}_{DSM-1}, \boldsymbol{P}_{DSM-2}, \ldots, \boldsymbol{P}_{OD}\right) \end{aligned} \tag{4}$$

From the vector $\boldsymbol{\mathcal{X}}_0$, a set of $2N+1$ initial *sigma points* is created : $\left[\boldsymbol{\mathcal{X}}_0^0, \ldots, \boldsymbol{\mathcal{X}}_0^j, \ldots, \boldsymbol{\mathcal{X}}_0^{2N}\right]$. These, following the unscented transformation derivation, are computed as:[29]

$$\begin{aligned} \boldsymbol{\mathcal{X}}_0^0 &= \overline{\boldsymbol{\mathcal{X}}}_0 && \text{for } j = 0 \\ \boldsymbol{\mathcal{X}}_0^j &= \boldsymbol{\mathcal{X}}_0^0 + \left[\sqrt{(N+\lambda)\,\boldsymbol{\mathcal{P}}_0}\right]_j && \text{for } j = 1 \to N \\ \boldsymbol{\mathcal{X}}_0^j &= \boldsymbol{\mathcal{X}}_0^0 - \left[\sqrt{(N+\lambda)\,\boldsymbol{\mathcal{P}}_0}\right]_{j-N} && \text{for } j = N+1 \to 2N \end{aligned} \tag{5}$$

where $[\cdot]_i$ extracts the i-th column vector of the matrix, and $\lambda = 0$ is a constant for the UT propagation method. With a nonlinear map $\boldsymbol{\mathcal{F}}$, the set of sigma points is propagated forward up to final time t_n:

$$\boldsymbol{\mathcal{X}}_n^j = \boldsymbol{\mathcal{F}}\left(\boldsymbol{\mathcal{X}}_0^j\right) \quad \text{for } j = 0 \to 2N \tag{6}$$

The nonlinear mapping takes into account both the propagation of the dynamics through the equations of motion (see Eq. (1)), and the effects of the uncertainty on the maneuvers. The definition of $\boldsymbol{\mathcal{F}}$ is recursive:

$$\boldsymbol{\mathcal{X}}_k^j = \begin{bmatrix} \boldsymbol{x}_k^j \\ \vdots \\ \Delta\boldsymbol{v}_{DSM-k}^j \\ \vdots \\ \boldsymbol{\varepsilon}_{OD}^j \end{bmatrix} = \boldsymbol{\mathcal{F}}\left(\boldsymbol{\mathcal{X}}_{k-1}^j\right) = \begin{bmatrix} \boldsymbol{\mathcal{F}}_{\boldsymbol{x}}\left(\boldsymbol{x}_{k-1}^j\right) \\ \vdots \\ \Delta\boldsymbol{v}_{DSM-k}^j \\ \vdots \\ \boldsymbol{\varepsilon}_{OD}^j \end{bmatrix} \tag{7}$$

where $\boldsymbol{\mathcal{F}}_{\boldsymbol{x}}$ is defined recursively as:

$$\begin{aligned} \boldsymbol{x}_k^j &= \boldsymbol{\mathcal{F}}_{\boldsymbol{x}}\left(\boldsymbol{x}_{k-1}^j\right) \\ &= \left\{ \begin{array}{ll} \boldsymbol{\varphi}\left(\boldsymbol{x}_{k-1}^j, t_{k-1}, t_k\right) + \left[\boldsymbol{0}, \Delta\boldsymbol{v}_{DSM-k}^j\right]^T & \text{if } j = 0 \\ \boldsymbol{\varphi}\left(\boldsymbol{x}_{k-1}^j, t_{k-1}, t_k\right) + \left[\boldsymbol{0}, \Delta\boldsymbol{v}_{DSM-k}^j\right]^T + \left[\boldsymbol{0}, \Delta\boldsymbol{v}_{TCM-k}^j\right]^T & \text{if } j \neq 0 \end{array} \right\} \end{aligned} \tag{8}$$

The definition of $\boldsymbol{\mathcal{F}}$ allows to propagate the sigma point for the states $\boldsymbol{x}_k^j$ in time, while keeping constant the sigma points of the DSMs, $\Delta\boldsymbol{v}_{DSM-k}^j$, and of the navigation error, $\boldsymbol{\varepsilon}_{OD}^j$. In addition, the evolution of the central sigma point is the nominal trajectory, as the nominal DSM is considered, $\Delta\boldsymbol{v}_{DSM-k}^0$, and the TCM is not applied. On the contrary, the evolution of the external sigma points are the true dispersed trajectories, which contain all sources of errors. Finally, TCMs are computed according to the differential guidance (see Eq. (3)). The differential guidance matrix $\boldsymbol{G}_k$ multiplies the closed-loop error for each sigma point, given by the difference between the estimate of the true state, $\hat{\boldsymbol{x}}_k^j$, and the nominal one, $\boldsymbol{x}_k^0$:

$$\Delta\boldsymbol{v}_{TCM-k}^j = \boldsymbol{G}_k\left(\hat{\boldsymbol{x}}_k^j - \boldsymbol{x}_k^0\right) \tag{9}$$

The estimated state is the propagation through the cut-off time of the result of the orbit determination process $\boldsymbol{x}_{OD,k}^j$ at time t_k, plus the nominal DSM:

$$\hat{\boldsymbol{x}}_k^j = \boldsymbol{\varphi}\left(\boldsymbol{x}_{OD,k}^j, t_{OD,k}, t_k\right) + \left[\boldsymbol{0}, \Delta\boldsymbol{v}_k^0\right]^T \tag{10}$$

where $\boldsymbol{x}_{OD,k}^{j}$ is given by the true state at the time of orbit determination, $t_{OD,k}$, plus the sigma point for the navigation error:

$$\boldsymbol{x}_{OD,k}^{j} = \boldsymbol{\varphi}\left(\boldsymbol{x}_{k-1}^{j}, t_{k-1}, t_{OD,k}\right) + \boldsymbol{\varepsilon}_{OD}^{j} \tag{11}$$

Finally, the mean value and covariance of the states at time t_k are computed with UT sample mean and covariance formulas:

$$\overline{\boldsymbol{x}}_k = \sum_{j=0}^{2N} w^j \boldsymbol{x}_k^j \tag{12}$$

$$\boldsymbol{P}_k = \sum_{j=0}^{2N} w^j \left(\boldsymbol{x}_k^j - \overline{\boldsymbol{x}}_k\right)\left(\boldsymbol{x}_k^j - \overline{\boldsymbol{x}}_k\right)^T \tag{13}$$

where the UT weights are: $w^0 = \dfrac{\lambda}{N+\lambda}$ and $w^j = \dfrac{1}{2\left(N+\lambda\right)}$ for $j = 1 \to 2N$.

The methodology developed in this work improves upon previous implementation of the unscented transformation for stochastic optimization.[8–11] Indeed, unlike previous works, where a resampling of sigma points was needed at each maneuvering time, this method continuously propagates sigma points without resampling, allowing the nonlinear dynamics to modify the distribution freely. This avoids the assumption that the distribution remains normal and provides more accurate and realistic trajectory data, as the propagated trajectories do not have jumps related to the resampling of the sigma points. Moreover, here the focus is directly on the realizations of the trajectory itself, i.e., the sigma points, and not on the mean trajectory and its covariance, as in previous research. As a consequence, the method also enables clearer differentiation between nominal and dispersed trajectories, facilitating smoother post-processing and eliminating the need for additional adjustments.

Statement of the Problem

In this section, the stochastic optimization problem is formulated as a NLP problem. The NLP vector $\boldsymbol{y}$ contains all the optimizing variables. In the case of LUMIO these are:

$$\boldsymbol{y} = \left[\Delta\boldsymbol{v}_{DSM-1}, \ldots, \Delta\boldsymbol{v}_{DSM-k}, \ldots, \Delta\boldsymbol{v}_{DSM-n}, t_0, \ldots, t_k, \ldots, t_n\right]^T \tag{14}$$

The nominal initial condition, $\boldsymbol{x}_0^0$, is left outside as it is fixed for LUMIO, but for other optimization problems it can be added with little modification. The objective function is defined as the sum of the deterministic and stochastic cost:

$$\begin{aligned} f &= \Delta V_{det} + \Delta V_{sto} \\ &= \sum_{k=1}^{n} \|\Delta\boldsymbol{v}_{DSM-k}^0\| + \overline{\Delta v}_{TCM} + 3\sigma_{\Delta v_{TCM}} \\ &= \sum_{k=1}^{n} \|\Delta\boldsymbol{v}_{DSM-k}^0\| + \sum_{j=0}^{2N} w^j \left(\sum_{k=1}^{n} \|\Delta\boldsymbol{v}_{TCM-k}^j\|\right) + \\ &+ 3\sqrt{\sum_{j=0}^{2N} w^j \left(\sum_{k=1}^{n} \|\Delta\boldsymbol{v}_{TCM-k}^j\| - \overline{\Delta v}_{TCM}\right)^2} \end{aligned} \tag{15}$$

where ΔV_{det} is the sum of the norms of each DSM, while ΔV_{sto} is the 3σ value of the sum of the norms of each TCM, computed as the mean value $\overline{\Delta v}_{TCM}$ plus 3 times the standard deviation $\sigma_{\Delta v_{TCM}}$; these are, in turn, computed with the UT weighted sample mean and covariance formulas. This definition of the objective function allows the optimizer to reach an overall optimal solution, as both the deterministic and stochastic cost are minimized. Finally, constraints are considered. Since the method allows to define a nominal trajectory, all usual constraints can be conventionally applied to the nominal trajectory, without modifying them. The nominal constraints for LUMIO, $\boldsymbol{c}_{nom}$, are:

$$\boldsymbol{c}_{nom} = \left\{ \begin{array}{c} \boldsymbol{x}_n^0 = \boldsymbol{x}_{qh}\left(t_n\right) \\ t_0 = \tilde{t}_0 \\ t_1 \geq t_0 + 6.5 \\ t_k \geq t_{k-1} + 3 \quad \text{for } k = 2 \rightarrow n \end{array} \right\} \tag{16}$$

In particular, the final nominal state, $\boldsymbol{x}_0^n$, is constrained to be equal to the state on the quasi-halo target orbit at final time t_n, as the presence of the HIM is taken into account in the propagation map $\boldsymbol{\mathcal{F}}$. The initial nominal state, $\boldsymbol{x}_0^0$, is implicitly fixed in the propagation itself, so no constraints are necessary, while the initial time, t_0, is constrained to be the release epoch $\tilde{t}_0$. The first maneuvering time, t_1, is at least 6.5 days after the release, while following maneuvering times are at least 3 days apart from each other, to allow 1 day of orbit determination and 2 days of cut-off time. Finally, to make sure that also dispersed trajectories reach the vicinity of the target, the final covariance is controlled: an upper boundary on the trace of the position and velocity covariance sub-matrices is imposed. This is called the covariance constraint, $\boldsymbol{c}_{cov}$, and it is defined as:

$$\boldsymbol{c}_{cov} = \left\{ \begin{array}{c} \text{tr}\left(\boldsymbol{P}_n^{rr}\right) \leq \tilde{\sigma}_r^2 \\ \text{tr}\left(\boldsymbol{P}_n^{vv}\right) \leq \tilde{\sigma}_v^2 \end{array} \right\} \tag{17}$$

where $\text{tr}\left(\cdot\right)$ is the trace operator, $\boldsymbol{P}_n^{rr}$ and $\boldsymbol{P}_n^{vv}$ are the covariance sub-matrices for position and velocity, respectively, and $\tilde{\sigma}_r$ and $\tilde{\sigma}_v$ are the standard deviation upper boundaries for position and velocity. Therefore, the stochastic optimization problem can be formulated as an NLP problem:

$$\min_{\boldsymbol{y}} \; f\left(\boldsymbol{y}\right) \text{ s.t. } \left\{ \begin{array}{c} \boldsymbol{c}_{nom} \\ \boldsymbol{c}_{cov} \end{array} \right\} \tag{18}$$

NUMERICAL ANALYSIS

The NLP problem in Eq. (18) is solved using MATLAB *fmincon*, with the *active-set* algorithm.[30,31] Analytical derivatives are provided to the optimizer, to smooth the solution of the problem. As initial guesses, the results of the LUMIO mission analysis are used. In particular, nominal trajectories are considered, together with their relative navigation assessment. These initial guesses will be referred to as the *deterministic optimization*, while the solution of the problem will be referred to as the *stochastic optimization*. The uncertainty on the initial conditions and the maneuver execution errors are the same presented before for LUMIO mission analysis. For the navigation errors, representative values from the knowledge analysis are used. The 1σ OD error for position and velocity is taken as 0.1 km and 0.5 mm/s, respectively. These values can be inferred by looking at Figure 3, and considering the mean value for the knowledge at the end of each OD phase. The upper limits for the final covariance are a standard deviation of 1 km for position and of 1 cm/s for velocity. These values are chosen so that the injection into the quasi-halo orbit has a lower dispersion, which results in lower station-keeping costs. In Table 2, all the relevant data used in the stochastic optimization are reported together for convenience.

Table 2: Data used for the Stochastic Optimization of LUMIO Trajectories

Data	1σ
Initial Position Dispersion	$100\ \mathrm{km}$
Initial Velocity Dispersion	$5\ \mathrm{cm/s}$
Maneuver Magnitude Error	2%
Maneuver Pointing Angle Error	$1.5\ \mathrm{deg}$
Position Navigation Error	$0.1\ \mathrm{km}$
Velocity Navigation Error	$0.5\ \mathrm{mm/s}$
Final Position Covariance Constraint	$1\ \mathrm{km}$
Final Velocity Covariance Constraint	$1\ \mathrm{cm/s}$

Results

This section reports the results of the stochastic optimization on trajectories with ID #02, #11, #20, #43, #48 and #51. In Table 3, for each trajectory, the deterministic, stochastic and total ΔV are reported together with the final position and velocity dispersion, $\sigma_r\left(t_n\right)$ and $\sigma_v\left(t_n\right)$. Values are reported both for the deterministic optimization only, and the stochastic optimization approach, for which the previous is used as initial guess.

Table 3: Results of the Stochastic Optimization Problem.

Traj. ID		ΔV_{det} [m/s]	ΔV_{sto} [m/s]	ΔV_{tot} [m/s]	$\sigma_r\left(t_n\right)$ [km]	$\sigma_v\left(t_n\right)$ [cm/s]
#02	Det. Opt.	47.24	20.22	67.46	12.49	6.44
	Sto. Opt.	49.64	9.44	59.08	1.00	0.58
#11	Det. Opt.	9.66	10.05	19.72	7.18	3.02
	Sto. Opt.	9.93	10.02	19.95	0.95	1.00
#20	Det. Opt.	42.92	16.04	58.96	4.57	3.31
	Sto. Opt.	44.15	8.57	52.72	1.00	0.51
#43	Det. Opt.	29.96	13.07	43.03	6.64	2.91
	Sto. Opt.	31.08	8.29	39.37	0.98	0.75
#48	Det. Opt.	41.82	18.41	60.23	6.01	2.92
	Sto. Opt.	43.84	9.06	52.90	0.93	0.76
#51	Det. Opt.	17.90	12.14	30.04	10.28	4.66
	Sto. Opt.	19.74	5.98	25.72	1.00	0.72

As it can be seen from Table 3, the stochastic optimization process is able to reduce considerably the total ΔV for the transfer, while also reducing the final covariance under the imposed limit. In particular, the reduction of ΔV is due to the decrease in the stochastic ΔV, i.e., the TCM cost, while the deterministic ΔV slightly increases. This happens for each trajectory except trajectory #11 where the optimization produces a solution with similar total ΔV as the initial guess, but reduces the final dispersion. In general, it seems that the process is able to obtain less expensive and, at the same, more robust trajectories. To understand how the optimization achieves this, let us use trajectory #20, the LUMIO baseline, as a representative example. A complete maneuvers breakdown and analysis is reported in Table 4: for each maneuver, the respective time of flight, the ΔV of the DSM, if any, and the ΔV of the TCM, as the 3σ value, are reported. It can be seen that

the optimization reduces the cost of each TCM, which causes the high reduction in the stochastic ΔV seen in Table 3. It is important to note that the optimization does not directly act on the TCM ΔV, which is given by the differential guidance, but it rather moves the maneuver time, as it can be seen in the time of flight column. This indirectly reduces the ΔV. In particular, for each trajectory, the first TCM is positioned as soon as possible, i.e., 6.5 days after t_0, to counteract the effects of the initial dispersion. Moreover, the TCM following a DSM is often placed after 3 days, which is the minimum maneuver distance, so that the dispersion coming from the erroneous DSM can be fixed as soon as possible. These 2 behaviours on the TCM timing are reasonable and could have been expected even before the stochastic optimization was performed. On the other hand, this proves the good performance of the optimization. Regarding other TCMs instead, the behaviour of the optimizer is more unpredictable. Indeed, a TCM can be anticipated or postponed with respect to the initial guess, without an evident reason. This suggests that the optimizer is able to chose the optimal TCM timing so that the total ΔV is minimized, which is the objective of the optimization itself. Regarding the DSMs, the optimizer is able to directly act on both the maneuver magnitude and timing. However, the timing and the magnitude are just slightly adjusted with respect to the initial guess, without a huge modification. The only deterministic maneuver which is highly modified is the HIM, which, in the case of trajectory #20, is performed ~ 3 days before, and its ΔV passes from 0.32 to 1.47 $\mathrm{m/s}$. This behaviour is common to all trajectories and it is what causes the increment on the deterministic ΔV. Moving the HIM timing is expected to make the deterministic ΔV increase, as the optimal HIM time was already chosen by the deterministic optimization. Still, the optimizer decides to always anticipate the maneuver. This can be explained by looking at Figure 6, where the position and velocity dispersion analysis of trajectory #20 are reported, both for the initial guess and the solution, i.e., the deterministic and the stochastic optimization. From the figure, it is possible to appreciate how the evolution of the dispersion, in the stochastic optimization case, is always more limited with respect to the deterministic only optimization. This shows how the optimal placement of the TCMs is able to reduce the dispersion, as well as the ΔV, as explained before. In addition, by looking at the final part of the transfer it is possible to see that the HIM is anticipated to match the constraint on the position and velocity covariance, which is represented with the dashed red line, In other words, the optimizer trades some of the deterministic ΔV to have less dispersion, and, hence, a more robust transfer.

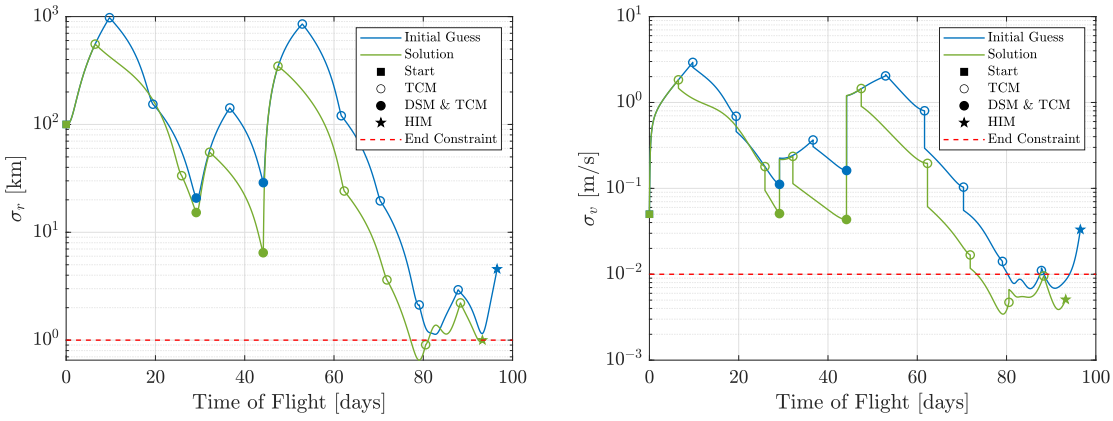

(a) 1σ Position Dispersion

(b) 1σ Velocity Dispersion

Figure 6: Trajectory #20: Dispersion Analysis

Table 4: Trajectory #20: Maneuvers Analysis.

Maneuver ID	Time of Flight [days]	ΔV_{DSM} [m/s]	ΔV_{TCM} (3σ) [m/s]
Deterministic Optimization			
#1	9.71	–	8.82
#2	19.43	–	3.16
#3	29.14	6.61	0.44
#4	36.66	–	1.26
#5	44.17	35.99	0.58
#6	52.90	–	6.55
#7	61.63	–	2.70
#8	70.36	–	0.38
#9	79.08	–	0.06
#10	87.81	–	0.06
#11	96.54	0.32	–
Stochastic Optimization			
#1	6.50	–	5.75
#2	25.88	–	0.69
#3	29.13	6.47	0.16
#4	32.13	–	0.80
#5	44.14	36.20	0.14
#6	47.45	–	4.44
#7	62.29	–	0.67
#8	71.86	–	0.07
#9	80.54	–	0.02
#10	88.32	–	0.05
#11	93.25	1.47	–

To sum up the findings on the stochastic optimization results, the following can be said:

- The stochastic optimization is successful, as it produces trajectories which require less fuel, and are, at the same time, more robust.
- This is achieved by reducing the total ΔV and the dispersion of the transfer.
- The optimizer is able to chose an optimal timing for each TCM, which highly reduces the stochastic part of the ΔV.
- The optimizer anticipates the halo insertion maneuver to match the final covariance constraint and gain more robustness, at the expense of a small increase on the deterministic part of the ΔV (which, nonetheless, is overcompensated by the savings on the stochastic part).

Monte Carlo Validation

In this section the results of the stochastic optimization, in terms of total ΔV and dispersion analysis, are validated with Monte Carlo (MC) simulations. In particular, the Monte Carlo analysis directly runs on the optimized trajectory, using the same uncertainties as for the UT propagation map. This means that for each sample of the MC run, the initial conditions, the error on the DSMs,

and the navigation errors are drawn randomly from their relative Gaussian distributions. In addition, to make it even more realistic, process noise is injected in the dynamics as a Gauss–Markov process, as it was done for LUMIO mission analysis. Again, the residual acceleration and the solar radiation pressure are considered. Their characteristics, in terms of standard deviation, σ, and correlation time, τ, are reported in Table 1.

For brevity, only results on trajectory #20 are shown here, as they are representative of the general behavior of the Monte Carlo analyses performed also on the other trajectories. An analysis with 10000 samples was performed, and, as it can be seen in Table 5, results show good accordance with the unscented transformation propagation. Indeed, the total ΔV predicted by UT is only $\sim 0.5\%$ smaller than the one obtained with the MC run, computed considering the 99.73 percentile. Similarly, the final position and velocity standard deviations predicted by UT are very close to the ones obtained with the MC run. There is a slight underestimation by UT, but this is deemed more than acceptable if one consider that no process noise is considered in the UT case. The full comparison between the UT and MC dispersion evolution is reported in Figure 7. It is clear that the two different approaches manage to get the same dispersion evolution, with a slight difference only on the final part of the transfer, when the dispersion is minimum. In addition, this portion of the transfer is very close to the quasi-halo orbit, where it is probable that the nonlinearity of the dynamics makes the effect of the process noise more relevant, which would explain the difference. However, if one looks at the absolute error between the UT prediction and the MC simulation, in Figure 8, it is clear that the difference is very small, less than $1\ \mathrm{km}$ for position and $3\ \mathrm{mm/s}$ for velocity, in the final section of the transfer. The biggest difference is, instead, in the initial portion, before the first TCM, where the UT actually overestimates the dispersion by $\sim 3\ \mathrm{km}$ for position and $\sim 1\ \mathrm{cm/s}$ for velocity. Then, as soon as the first TCM is applied, the difference drops close to zero. It is important to note that, for mission analysis purposes, these kinds of differences are negligible. Finally, the complete position distribution at the final time, i.e., the time of the halo insertion, is shown in Figure 9. The color map describes the probability density, where lighter colors mean more probability that the final position is in that region. The distribution appears to still be very close to the normal one, as the 3σ covariance ellipsoid predicted by the UT shows.

Table 5: Monte Carlo Analysis Results on Trajectory #20

	ΔV_{tot} [m/s]	$\sigma_r\,(t_n)$ [km]	$\sigma_v\,(t_n)$ [cm/s]
UT (without Process Noise)	52.72	1.00	0.51
MC (with Process Noise)	53.01	1.02	0.66

CONCLUSION

In this work a method for stochastic trajectory optimization under uncertainty is developed. All the main sources of uncertainty are considered. A new implementation of the unscented transformation is proposed, where a nonlinear map propagates continuously trajectories and uncertainties, without the need of resampling sigma points at any step. This avoids simplifications in assuming that the distribution remains normal, and allows the direct optimization of the nominal and dispersed trajectories. With the proposed propagation, the stochastic optimization problem is converted into a deterministic nonlinear programming problem, which can be solved with conventional techniques. The objective function takes into account both the deterministic ΔV, coming from the nominal maneuvers, and the stochastic ΔV, from the correction maneuvers. These are computed considering the differential guidance. Conventional constraints can be applied to the nominal trajectory,

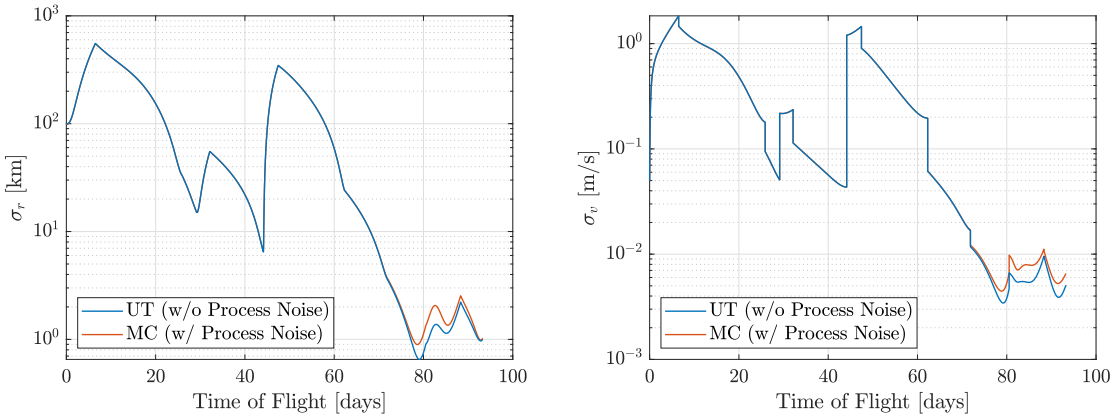

(a) 1σ Position Dispersion

(b) 1σ Velocity Dispersion

Figure 7: Dispersion Analysis: Comparison between UT and MC

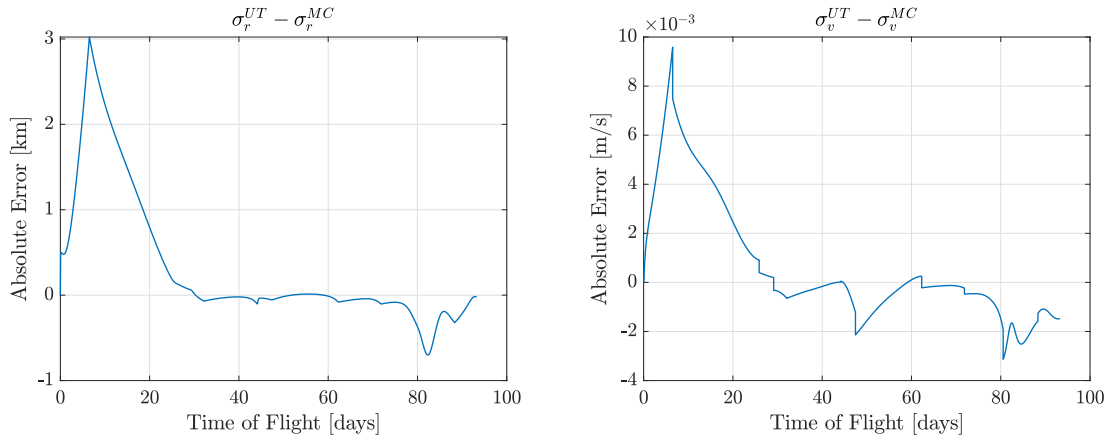

(a) Position Dispersion Error

(b) Velocity Dispersion Error

Figure 8: Dispersion Analysis: Error between UT and MC

while stochastic constraints on the final covariance are imposed to limit the final dispersion. The method is tested on 6 WSB transfer trajectories, using the LUMIO mission as a test case. This constitutes a new and challenging application for stochastic optimization methods. The results show that the method is able to produce trajectories which require less fuel, and, at the same time, are more robust, if compared to conventional deterministic optimization techniques. In particular, both the total ΔV and the final dispersion are reduced, while an optimal placement in time of correction maneuvers is achieved. Finally, results are validated with Monte Carlo analyses, which show good agreement with the unscented transformation predictions, both in terms of fuel cost and dispersion evolution. Future research might improve upon these results by considering other types of guidance for correction maneuvers, which could further enhance the optimization process.

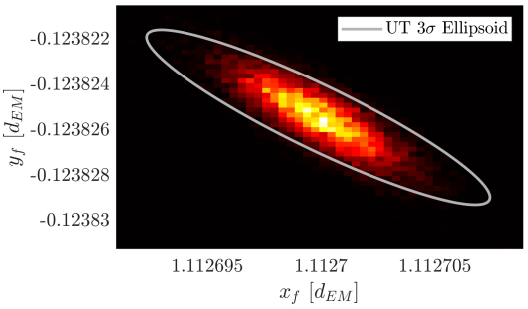

(a) xy Distribution

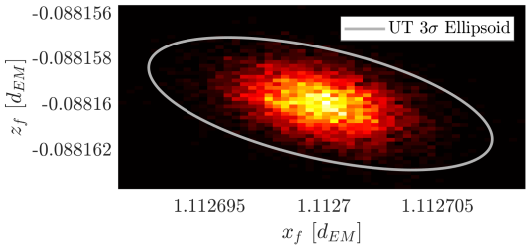

(b) xz Distribution

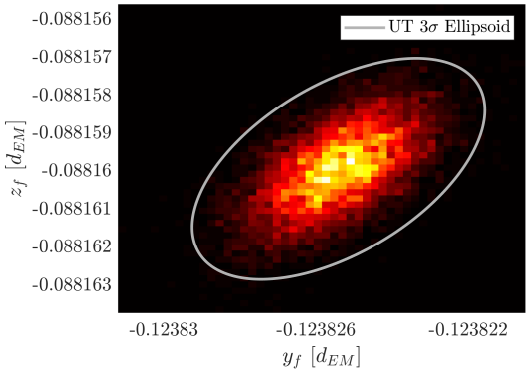

(c) yz Distribution

Figure 9: Final Position Distribution: MC Probability Density Plot and UT 3σ Prediction

ACKNOWLEDGMENT

Part of the work described in this paper has been funded by the European Space Agency under the General Support Technology Programme (GSTP), ESA contract No. 4000139301/22/NL/AS, and has received support from the national delegations of Italy (through ASI's ALCOR program) and Norway.

REFERENCES

[1] C. Giordano, *Analysis, Design, and Optimization of Robust Trajectories for Limited-Capability Small Satellites*. PhD thesis, Politecnico di Milano, 2020.

[2] W. Fehse, *Automated Rendezvous and Docking of Spacecraft*. Cambridge Aerospace Series, Cambridge University Press, 2003, https://doi.org/10.1017/CBO9780511543388.

[3] A. Poghosyan and A. Golkar, "CubeSat evolution: Analyzing CubeSat capabilities for conducting science missions," *Progress in Aerospace Sciences*, Vol. 88, 2017, pp. 59–83, https://doi.org/https://doi.org/10.1016/j.paerosci.2016.11.002.

[4] E. A. Belbruno and J. K. Miller, "Sun-Perturbed Earth-to-Moon Transfers with Ballistic Capture," *Journal of Guidance, Control, and Dynamics*, Vol. 16, No. 4, 1993, pp. 770–775, https://doi.org/10.2514/3.21079.

[5] J. T. Betts, "Survey of Numerical Methods for Trajectory Optimization," *Journal of guidance, control, and dynamics*, Vol. 21, No. 2, 1998, pp. 193–207, https://doi.org/10.2514/2.4231.

[6] Y. Z. Luo and Z. Yang, "A review of uncertainty propagation in orbital mechanics," *Progress in Aerospace Sciences*, Vol. 89, 2017, pp. 23–39, https://doi.org/10.1016/j.paerosci.2016.12.002.

[7] S. Kelly and D. Geller, "Robust Cislunar Trajectory Optimization in the Presence of Stochastic Errors," *The Journal of the Astronautical Sciences*, Vol. 71, No. 4, 2024, p. 30, https://doi.org/10.1007/s40295-024-00450-x.

[8] N. Marmo and A. Zavoli, "Chance-constraint optimization of interplanetary trajectories with a hybrid multiple-shooting approach," *2022 AAS/AIAA Astrodynamics Specialist Conference*, Charlotte, NC, 2022.

[9] N. Marmo, A. Zavoli, N. Ozaki, and Y. Kawakatsu, "A hybrid multiple-shooting approach for covariance control of interplanetary missions with navigation errors," *33rd AAS/AIAA Space Flight Mechanics Meeting*, Austin, TX, 2023.

[10] N. Ozaki, S. Campagnola, and R. Funase, "Tube Stochastic Optimal Control for Nonlinear Constrained Trajectory Optimization Problems," *Journal of Guidance, Control, and Dynamics*, Vol. 43, No. 4, 2020, pp. 645–655, https://doi.org/10.2514/1.G004363.

[11] K. Oguri and J. W. McMahon, "Robust Spacecraft Guidance Around Small Bodies Under Uncertainty: Stochastic Optimal Control Approach," *Journal of Guidance, Control, and Dynamics*, Vol. 44, No. 7, 2021, pp. 1295–1313, https://doi.org/10.2514/1.G005426.

[12] J. Ridderhof, J. Pilipovsky, and P. Tsiotras, "Chance-constrained covariance control for low-thrust minimum-fuel trajectory optimization," *2020 AAS/AIAA Astrodynamics Specialist Conference*, South Lake Tahoe, CA, 2020, pp. 9–13.

[13] C. Giordano and F. Topputo, "Analysis, Design, and Optimization of Robust Trajectories in Cislunar Environment for Limited-Capability Spacecraft," *The Journal of the Astronautical Sciences*, Vol. 70, No. 6, 2023, p. 53, https://doi.org/10.1007/s40295-023-00413-8.

[14] C. Greco, S. Campagnola, and M. Vasile, "Robust Space Trajectory Design Using Belief Optimal Control," *Journal of Guidance, Control, and Dynamics*, Vol. 45, No. 6, 2022, pp. 1060–1077, https://doi.org/10.2514/1.G005704.

[15] X. Fu, N. Baresi, and R. Armellin, "Stochastic optimization for stationkeeping of periodic orbits using a high-order Target Point Approach," *Advances in Space Research*, Vol. 70, No. 1, 2022, pp. 96–111, https://doi.org/10.1016/j.asr.2022.04.039.

[16] F. Topputo, G. Merisio, V. Franzese, C. Giordano, M. Massari, G. Pilato, D. Labate, A. Cervone, S. Speretta, A. Menicucci, E. Turan, E. Bertels, J. Vennekens, R. Walker, and D. Koschny, "Meteoroids detection with the LUMIO lunar CubeSat," *Icarus*, Vol. 389, 2023, https://doi.org/10.1016/j.icarus.2022.115213.

[17] A. M. Cipriano, D. A. D. Tos, and F. Topputo, "Orbit Design for LUMIO: The Lunar Meteoroid Impacts Observer," *Frontiers in Astronomy and Space Sciences*, Vol. 5, 2018, p. 29, https://doi.org/10.3389/fspas.2018.00029.

[18] C. Giordano, A. Martinelli, C. Buonagura, G. Merisio, V. Franzese, and F. Topputo, "Trajectory design and analysis of the LUMIO CubeSat," *AIAA Scitech 2024 Forum*, Orlando, FL, 2024, https://doi.org/10.2514/6.2024-1271.

[19] D. A. Dei Tos and F. Topputo, "On the advantages of exploiting the hierarchical structure of astrodynamical models," *Acta Astronautica*, Vol. 136, 2017, pp. 236–247, https://doi.org/10.1016/j.actaastro.2017.02.025.

[20] Gómez, G., Masdemont, J. J., and Mondelo, J. M., "Solar system models with a selected set of frequencies," *Astronomy & Astrophysics*, Vol. 390, No. 2, 2002, pp. 733–749, https://doi.org/10.1051/0004-6361:20020625.

[21] D. A. Dei Tos, "Automated Trajectory Refinement of Three-Body Orbits in the Real Solar System Model," Master's thesis, Politecnico di Milano, 2014.

[22] V. Szebehely, *Theory of orbit: The restricted problem of three Bodies*. Elsevier, 2012.

[23] W. M. Folkner, "Planetary ephemeris DE432," Interoffice Memorandum 392R-14-003, Jet Propulsion Laboratory, April 2014.

[24] C. H. Acton, "Ancillary data services of NASA's Navigation and Ancillary Information Facility," *Planetary and Space Science*, Vol. 44, No. 1, 1996, pp. 65–70. Planetary data system, https://doi.org/10.1016/0032-0633(95)00107-7.

[25] C. Acton, N. Bachman, B. Semenov, and E. Wright, "A look towards the future in the handling of space science mission geometry," *Planetary and Space Science*, Vol. 150, 2018, pp. 9–12. Enabling Open and Interoperable Access to Planetary Science and Heliophysics Databases and Tools, https://doi.org/10.1016/j.pss.2017.02.013.

[26] D. A. Dei Tos, M. Rasotto, F. Renk, and F. Topputo, "LISA Pathfinder mission extension: A feasibility analysis," *Advances in Space Research*, Vol. 63, No. 12, 2019, pp. 3863–3883, https://doi.org/10.1016/j.asr.2019.02.035.

[27] B. Schutz, B. Tapley, and G. H. Born, *Statistical Orbit Determination*. Elsevier, 2004, https://doi.org/10.1016/B978-0-12-683630-1.X5019-X.

[28] C. Giordano and F. Topputo, "A Hybrid Stochastic-Deterministic Integrator for Spacecraft Dynamics with Uncertainty," *33rd AAS/AIAA Space Flight Mechanics Meeting*, Austin, TX, 2023, pp. 1–23.

[29] S. Julier, J. Uhlmann, and H. Durrant-Whyte, "A New Approach for Filtering Nonlinear Systems," *Proceedings of 1995 American Control Conference - ACC'95*, Vol. 3, 1995, pp. 1628–1632 vol.3, https://doi.org/10.1109/ACC.1995.529783.

[30] M. Biggs, "Constrained Minimization Using Recursive Quadratic Programming," *Towards global optimization*, 1975.

[31] R. Fletcher, *Practical methods of optimization*. John Wiley & Sons, 1987, https://doi.org/10.1002/9781118723203.